Polymer xxx (2018) xxx-xxx

Contents lists available at ScienceDirect

Polymer

journal homepage: www.elsevier.com

Damage self-sensing behavior of carbon nanofiller reinforced polymer composites with different conductive network structures

Dong Xiang[a, *, 1], Lei Wang[a, 1], Yuhao Tang[a], Eileen Harkin-Jones[b], Chunxia Zhao[a], Ping Wang[a], Yuntao Li[a, **]

[a] School of Materials Science and Engineering, Southwest Petroleum University, Chengdu, 610500, China
[b] School of Engineering, University of Ulster, Jordanstown, BT37 0QB, UK

ARTICLE INFO

Keywords:
Carbon nanotube
Graphene nanoplatelet
Damage self-sensing
Conductive network structure
Polymer composites

ABSTRACT

Multi-walled carbon nanotube (MWCNTs) and graphene nanoplatelet (GNPs) filled high-density polyethylene (HDPE) composites with randomly dispersed (DCN) and segregated (SCN) conductive network structures were fabricated by a solution-assisted mixing method. The damage self-sensing behavior of the resulting composites was investigated via in situ electrical-mechanical measurements. The results show that nanofiller type and conductive network structure significantly influence the damage self-sensing behavior of the composites. The relative resistance change (RRC) of HDPE/MWCNT composites during tensile deformation can be divided into three stages. Compared to HDPE/MWCNT composites with DCN structures, more robust conductive networks are formed in SCN structures, resulting in smaller RRC. The self-damage sensing behavior of all HDPE/GNP composites follows a similar trend, starting with a quasi-linear increase in RRC followed by a sudden rise induced by brittle fracture of the material. Nanofiller content was also found to affect the damage self-sensing behavior of the composites with a higher nanofiller loading corresponding to a lower damage sensing sensitivity. A modeling study based on tunneling theory was also conducted to further analyze the mechanism. In addition, the tensile properties of the composites were measured. This study provides some important information for development of smart structural materials.

1. Introduction

Over the last decade, tremendous effort has been devoted to developing multifunctional composite materials by adding conductive fillers into polymer matrices [1–5]. At appropriate filler content, the resulting conductive polymer composites (CPCs) showed excellent electrical conductivities and considerable mechanical strength. These attributes were used to develop smart structural materials, including damage self-sensing (or damage self-monitoring) polymer composites able to provide structural and sensing properties [6–8]. The ability to detect damage in composite materials is extremely important and particularly in safety critical applications such as in the aerospace or automotive sectors. Therefore, studies that advance the ability to detect damage in composite structures are very important.

Nondestructive testing methods, such as X-ray [9], optical fiber [10] and acoustic emission sensor [11] have been widely used in damage sensing. However, most of these traditional monitoring techniques require embedding or attachment of the sensing elements. This, in turn, forms defects in the materials or requires large scale test equipment. Damage self-sensing techniques based on in situ electrical resistance measurements have been demonstrated to be an alternative to traditional techniques. The method is based on monitoring the changes in electrical current (or resistance) in the composite induced by transformation or disintegration of conductive networks under deformation.

Suitable candidates for conductive additives include metals (e.g., powder or fibers) and carbonaceous fillers (e.g., carbon black (CB), carbon fibers (CFs), carbon nanotubes (CNTs), and graphene nanoplatelets (GNPs)). Metal-based materials have the disadvantages of requiring relative large loadings and thus being heavier. The higher loadings also lead to reduction in processability and elevated costs [12]. Carbonaceous materials have outstanding electronic and mechanical properties combined with being lightweight. Therefore, they show considerable promise as conductive fillers in damage self-sensing composites [13–15]. CB is a traditional carbonaceous filler, extensively studied and modeled in the transformation and re-construction processes in conductive networks during strain elongation [16–18]. For instance, Zheng et al. [19] categorised the transformation of conductive pathways in HDPE/CB composites

* Corresponding author.
** Corresponding author.
Email addresses: dxiang01@hotmail.com (D. Xiang); yuntaoli@swpu.edu.cn (Y. Li)
[1] These authors contributed equally to this work.

https://doi.org/10.1016/j.polymer.2018.11.007
Received 29 August 2018; Received in revised form 28 October 2018; Accepted 3 November 2018
Available online xxx
0032-3861/

subjected to uniaxial tension into four steps and showed that the increase in electrical resistance is attributed to the physical separation of the CB particles. Carbon fibers (CFs) combine excellent tensile strength with high electrical conductivity and are often employed as structural reinforcing elements in thermosetting resins to give provide effective damage self-sensing properties [20–22].

More recently, CNTs and GNPs have attracted increasing attention due to their outstanding mechanical and electrical properties [23–25]. Due to their high aspect ratios efficient conductive networks can be constructed with low electrical percolation thresholds. Ke et al. [26] measured lower percolation threshold ($\emptyset_c = 0.53$ wt.%) values for polyvinylidene fluoride (PVDF)/CNT nanocomposites than that for a CB-filled composites ($\emptyset_c = 1.81$ wt.%). This was attributed to the higher aspect ratio and ability to form networks with CNTs. Graphene nanoplatelets with 2-dimensional structures also possess high intrinsic electrical conductivities but the strong Van der Waals forces induced by the large surface areas of GNPs promote their aggregation, making them difficult to uniformly disperse in the polymer matrix to form a conducting network. Consequently, polymer/GNP composites have been found to exhibit moderate electrical conductivities [27].

Nanni et al. [28] prepared extruded MWCNT/polyethylene terephthalate (PET) sheets and evaluated their damage self-sensing behavior. They concluded that filler loading and directional alignment of the MWCNTs considerably affected the self-sensing properties of the composites [29,30]. The distribution of conductive fillers in the matrix has been shown to have an influence on the electrical percolation threshold of nanocomposites with segregated conductive network (SCN) being shown to outperform dispersed conductive networks (DCN) [31–34]. For example, Lin et al. [35] measured a percolation value as low as 0.4 vol % in a natural rubber (NR)/graphene system with a SCN structure, which was an 8-fold reduction compared to that achieved with a dispersed conductive network (DCN). Other studies have confirmed this result [36,37].

In the present study we extend the knowledge in this field of self-sensing materials by examining the importance of the conductive network structure (DCN and SCN) on the damage sensing capability of nanocomposites made with GNPs and MWCNTs. Composites containing different contents of nanofillers were prepared by solution-assisted mixing to form various conductive network structures (SCN and DCN) of HDPE/MWCNT and HDPE/GNP nanocomposites. The damage self-sensing behavior and tensile properties of the composites were investigated by in situ monitoring of current changes during uniaxial tensile testing. The composites exhibited distinct self-sensing behaviors which were dependent on the type and content of the nanofiller and conductive network structure. The results also showed an increase in Young's modulus of the composites as more nanofillers were added.

2. Experimental section

2.1. Materials

Commercial HDPE powder (888LIB) with a melt flow index of 0.2 g 10 min^{-1} was supplied by Mitsui Chemical. Its average particle size is calculated to be 107.9 μm, and the particle size distribution is shown in Fig. S1. GNPs (xGNP-15) with average diameter of 15 μm and thickness of 6–8 nm were purchased from XG Science (USA). Its density is 2.2 g cm^{-3} and carbon content exceeds 99.5%. MWCNTs (NC-7000) with purity of 90%, density of 1.85 g cm^{-3}, typical diameter of 9.5 nm and average length of 1.5 μm were obtained from Nanocyl S.A. (Belgium). O-dichlorobenzene (o-DCB) and ethanol were both kindly provided by Chron Chemicals (Chengdu), and were used to dissolve HDPE and disperse the carbon nanofillers.

2.2. Composite preparation

HDPE/MWCNT and HDPE/GNP composites with segregated and dispersed conductive networks were prepared by a solution-assisted mixing method illustrated in Fig. 1. Firstly, appropriate amounts of MWCNTs or GNPs were dispersed in ethanol and o-DCB by ultrasonication at 100 W and 40 kHz for 1 h at ambient temperature. To form the segregated conductive network structure, HDPE powder was added to the nanofiller/ethanol suspension and stirred for 15 min followed by 1 h ultrasonication (Fig. 1a). To prepare the dispersed conductive network structure, HDPE powder was firstly dissolved in o-DCB under stirring at 130 °C and then cooled down to ambient temperature. Subsequently, the above nanofiller/o-DCB suspension was added to the mixture and quickly stirred for 1 h (Fig. 1b). The HDPE/nanofiller/solvent mixtures prepared by the two different routes were both pump filtrated and dried in a vacuum oven at 80 °C for 24 h to obtain the HDPE/nanofiller blends. Finally, the dried blends were compression molded into sheets ($76 \times 76 \times 1\ mm^3$) at 170 °C under 10 MPa for 10 min. The resulting composite samples were labelled as x-CNTy and x-GNPy, where x stands for composites with segregated (S) or dispersed (D) conductive network and y refers to the weight fraction of nanofillers (wt.%). S-GNP3 thus represents a HDPE composite with a segregated conductive network and 3 wt.% GNPs loading.

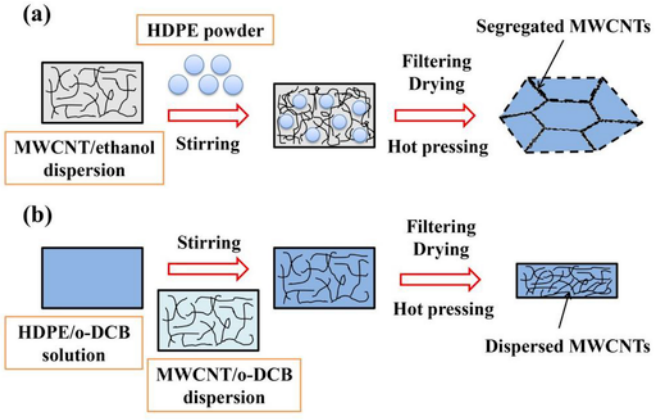

Fig. 1. A schematic representation of the preparation process of HDPE/MWCNT composites with (a) SCN and (b) DCN structures. The HDPE/GNP composites are prepared using the same method.

2.3. Characterization

The particle sizes and distribution of the as-received HDPE powder were characterised using a laser particle size analyzer (Malvern Mastersizer 2000). The fractured surface morphology of the composites was investigated via Scanning Electron Microscopy (ZEISS EV0 MA15) at an acceleration voltage of 20 kV. Cryo-fractured surfaces of specimens were permanganic etched [38] for 2 h with ultrasonication at 100 W to remove the amorphous phase of HDPE. The etched samples were then gold sputtered prior to imaging. The direct current (DC) electrical conductivity (σ_{DC}) values of the specimens were measured using the two-point method combined with a picoammeter (Keithley 6485) and DC voltage source (Tektronix PWS4323) at constant voltage of 3 V. The dimensions of the samples were $50 \times 10 \times 1\ mm^3$. Silver paint was used to minimize the contact resistance between samples and wires, and the distance of the coupled electrodes was set to 30 mm (Fig. 2a). The electrical conductivity values were calculated using the formula: $\sigma_{DC} = L/(R \times S)$, where R is the electrical resistance of the sample, and L and S are the length and cross-sectional area, respectively. Three specimens were used for each type of composite sample.

The damage self-sensing behavior of each nanocomposite was measured using a mechanical-electrical measurement system consisting of a universal testing machine (MTS CMT-4000), picoammeter, and DC voltage source (Fig. 2c). A voltage of 3 V was applied to the specimens and uniaxial tensile testing was carried out at a constant rate of 1 mm min^{-1}. Dumbbell samples (ASTM-D638) were obtained from the compression molded sheets and both sides were coated with silver paste prior to tensile testing (Fig. 2b). All electrical and mechanical data were collected by specialized software. Five specimens for each composite were tested and the average value was used for calculations.

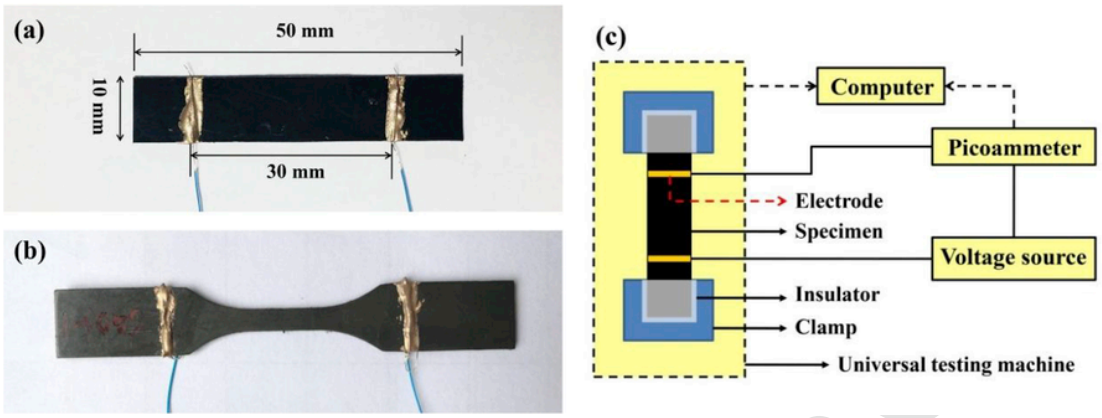

Fig. 2. Photographs of specimens for (a) electrical conductivity measurement and (b) in situ mechanical-electrical measurement. (c) A schematic representation of the mechanical-electrical measurement system.

X-ray diffraction analysis (XRD) was performed using a DX-2700 diffractometer to measure the crystallinity (X_{XRD}) of the composites after stretching to different strains. Cu-Kα radiation with a wavelength of 0.154 nm was used and data were recorded from 3 to 60°with a scanning speed of 0.03°min^{-1}. In addition, the orientation of the HDPE crystals was investigated using two-dimension wide-angle X-ray diffraction (2D-WAXD) measurements, which was conducted on a DISCOVER D8 diffractometer (Bruker). The X-ray wavelength was 0.154 nm by using Cu-Kα radiation. The samples were placed with the beam perpendicular to the stretching direction. The 2θ range covered was 0–35°. The orientation degrees were calculated from 1D diffraction profiles, which were integrated from 2D-WAXD patterns.

3. Results and discussion

3.1. Percolation and morphology

The volume conductivity of HDPE/MWCNT and HDPE/GNP composites with different network structures and related percolations are illustrated in Fig. 3. According to classical electrical percolation theory, conductive nanofillers will form numerous conductive pathways in insulating polymer matrices, leading to increased conductivities at nanofiller concentrations approaching the critical value [39]. As shown in Fig. 3, the composites exhibited clear percolation behavior. The effect of conductive network structures on the volume conductivity of each composite was quantitatively analyzed using a scaling law of percolation threshold (Equation (1)) [40].

$$\sigma_{DC} \propto (\emptyset - \emptyset_c)^t \quad (1)$$

where σ_{DC} is the electrical conductivity of the nanocomposite, $\emptyset$ is the filler weight fraction, $\emptyset_c$ is filler weight fraction at percolation threshold, and t represents the critical exponent depending on the dimensionality of conductive networks. The formula follows a power-law dependence of approximately 1.6–2.0 in a 3-dimensional system and 1.0–1.3 in a 2-dimensional system [41,42].

For the HDPE/MWCNT composites with a SCN structure, the lowest percolation threshold was obtained as $\emptyset_c$ = 0.1 wt.% (Fig. 3a). The related critical exponent of 1.70 indicates the formation of a typical 3-dimensional conductive network. By comparison, the HDPE/MWCNT composite with a DCN structure exhibits a higher percolation threshold ($\emptyset_c$ = 0.5 wt.%). The SEM image in Fig. 4a reveals that nanotubes mainly accumulate at the boundaries of the HDPE phase, forming dense, net-like conductive pathways. This structure (SCN) arises from directly hot compressing HDPE powder and MWCNTs into sheets, where nanotubes cannot efficiently diffuse into the HDPE matrix due to its high viscosity. Consequently, nanotubes build more close connections to form a more efficient conductive network in such a limited region.

For the HDPE/MWCNT composites with a DCN structure (Fig. 4b), nanotubes and their agglomerates are uniformly dispersed in the HDPE matrix. In this case, the MWCNTs are distributed over a much larger space and the DCN structure is therefore less efficient in electrical conduction than the SCN structure. In addition, One can observe in Fig. 3a that the D-CNT1 system exhibits a high critical exponent (t = 3.89), indicating that t may not be universal in some practical systems. For tunneling percolation systems, t values above 2 may be due to (1) addition of high aspect ratio conductive fillers (e.g., >50) and a low percolation threshold (e.g., <0.01); (2) a fundamental difference between lattice (universal three dimension lattice model [43]) and continuum percolation, where the latter may exhibit nonrandom contacts between particles associated with local orientational coupling of anisotropic units and distance dependent

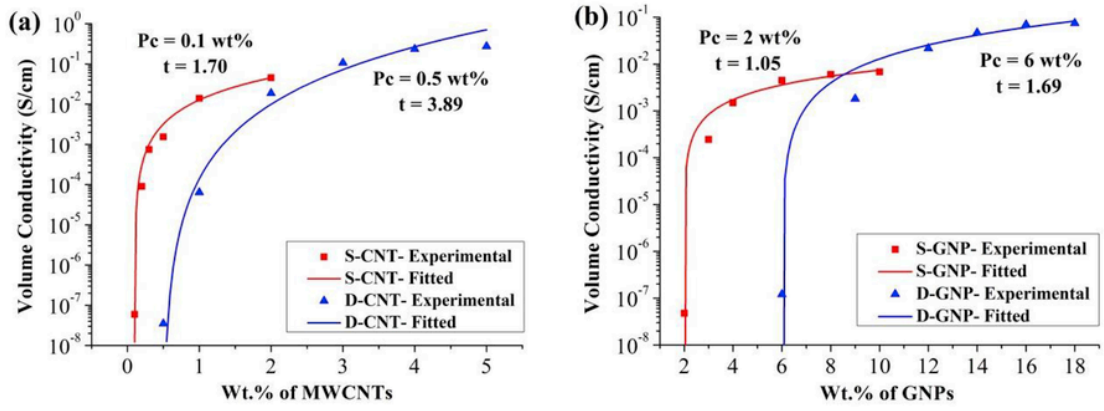

Fig. 3. Percolation curves of MWCNTs (a) and GNPs (b) filled composites with different conductive network structures.

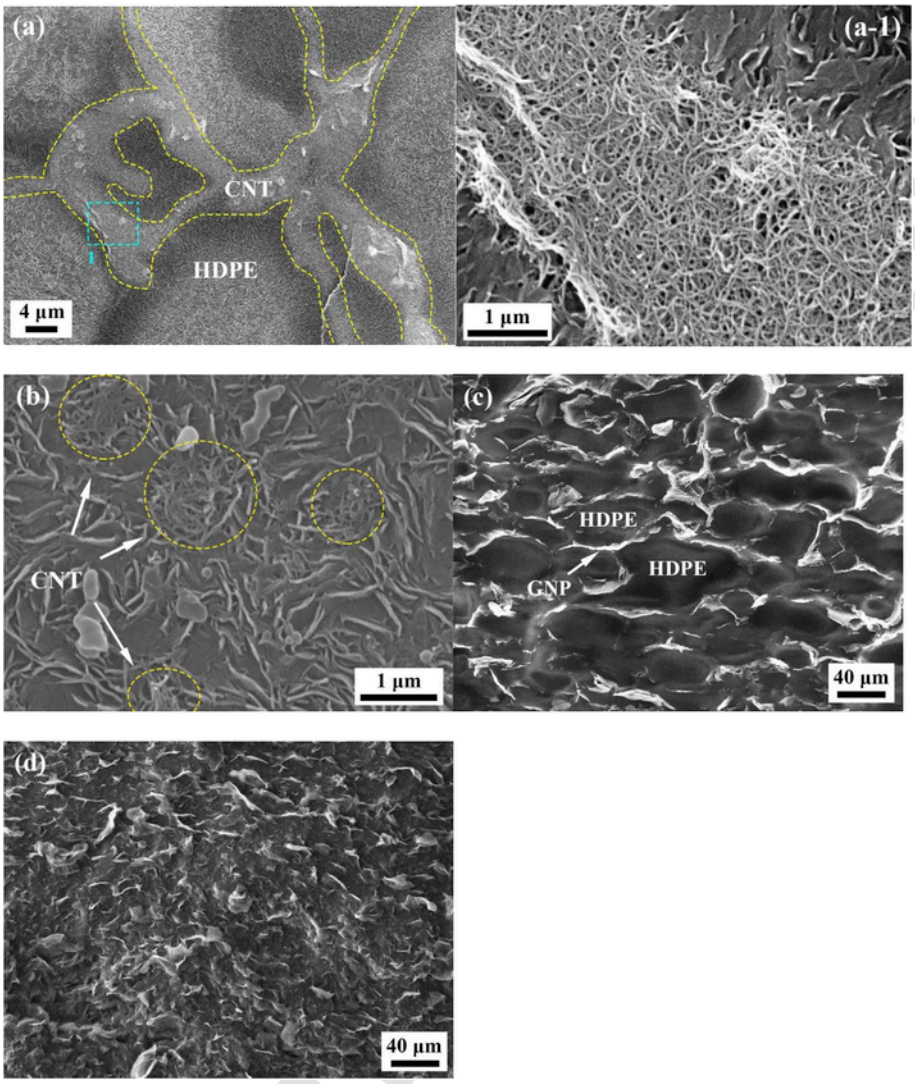

Fig. 4. SEM micrographs of HDPE composites with different nanofiller contents and conductive network structures: (a) S-CNT1, (b) D-CNT1, (c) S-GNP4, and (d) D-GNP12.

transport at the connections [44,45]. Numerous others have observed $t > 2$ in various disordered insulator/conductor systems [46–48].

With respect to GNP filled systems, the $\varnothing_c$ values were estimated to be 2.0 wt.% and 6.0 wt.% for HDPE/GNP composites with SCN and DCN structures, respectively (Fig. 3b). These values indicate that GNPs in the segregated structure also construct efficient conductive networks (Fig. 4c). Furthermore, the HDPE/GNP system with a DCN structure yields a 3-dimensional conductive network ($t = 1.69$) while that of the SCN structure is 2-dimensional ($t = 1.05$). In general, GNP filled composites have higher percolation thresholds ($\varnothing_c$) than HDPE/MWCNT systems, regardless of the network structure. The poorer enhancement in conductivity of composites may be attributed to the 2D flake-like shape of GNPs (Fig. 4d). Although several types of contact between GNPs exist in the polymer matrix, such as plane-to-plane, edge-to-edge and edge-to-plane, only the plane-to-plane contact would be beneficial for electrical transfer [49]. In addition, another possible reason can be the existence of some nonconductive graphene oxides and structural defects in the commercial GNPs used in this work.

3.2. Damage self-sensing behavior

In general, damage self-sensing behavior that depends on disruption of a conductive pathway requires operation around the percolation threshold ($\varnothing_c$) [50]. Conductive polymer composites with slightly higher loadings of nanofiller than the percolation threshold would be more desirable for practical applications to keep material costs down. Therefore, specimens with a nanofiller concentration just above $\varnothing_c$ were selected to investigate self-sensing behavior in this study. The conductive polymer composites used for damage self-sensing studies are listed in Table 1.

3.2.1. Damage self-sensing of HDPE/MWCNT composites

Fig. 5 illustrates the damage self-sensing behavior of the selected HDPE/MWCNT composites, where the relationship between stress and relative resistance change ($RRC = \Delta R/R_0$, Equation (2)) versus strain are presented.

Table 1
Details of the samples for damage self-sensing measurement.

Sample	Nanofiller type	Nanofiller loading [wt.%]	Network structure
S-CNT1	MWCNTs	1	SCN[a]
D-CNT1	MWCNTs	1	DCN[b]
D-CNT3	MWCNTs	3	DCN
S-GNP3	GNPs	3	SCN
S-GNP4	GNPs	4	SCN
D-GNP12	GNPs	12	DCN

[a] SCN: Segregated conductive network.
[b] DCN: Dispersed conductive network.

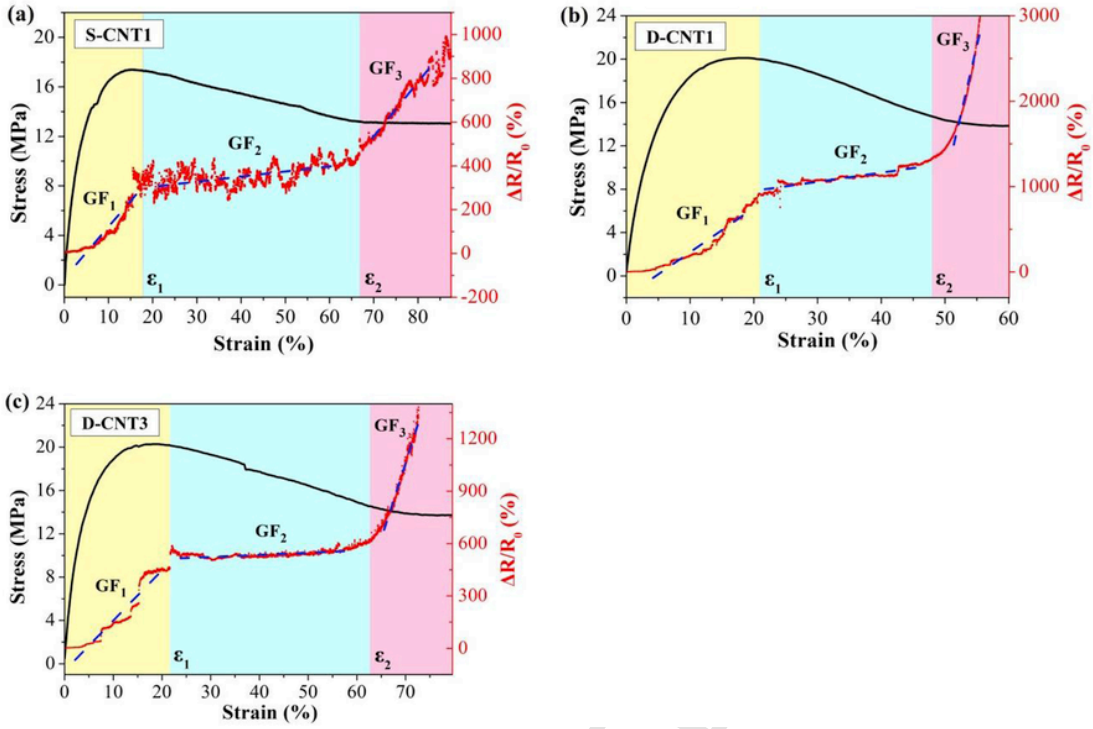

Fig. 5. Tensile stress and relative resistance change ($\Delta R/R_0$) as a function of strain in (a) S-CNT1, (b) D-CNT1, and (c) D-CNT3.

$$\frac{\Delta R}{R_0} = \frac{R - R_0}{R_0} \tag{2}$$

where R and R_0 are the real-time and initial electrical resistance, respectively.

The gauge factor (GF, Equation (3)) was applied to evaluate the resistance change sensitivity of the composites in Fig. 5, and the results are tabulated in Table 2.

$$GF = \frac{\Delta R/R_0}{\Delta \varepsilon} \tag{3}$$

where $\Delta\varepsilon$ represents the change in strain.

The damage self-sensing behavior of the HDPE/MWCNT composites is composed of three main stages: (1) prior to yielding, (2) strain softening and (3) necking growth. In the first stage (yellow background in Fig. 5a–c), all the $\Delta R/R_0$ curves increase with strain elongation until a plateau is reached. The turning points, denoted as ε_1, occur at a strain of around 20% (Table .2). These are closely aligned with the yielding points in the stress-strain curves.

In order to explain this phenomenon more clearly, the proposed deformation mechanism of the networks is shown in schematic form in Figs. 6 and 7. It is clear that the composites experience only a small deformation prior to yielding and both conductive network structures basically retain their original shapes. However, the distance between neighboring nanotubes or their agglomerates slightly increases. One can see in Fig. S2 that the X_{XRD} values of the polymer are 62.4% and 64.8% for D-CNT1 and S-CNT1 before stretching and there is little change when stretched up to ε_1. The orientation degree of the HDPE crystals in D-CNT1 and S-CNT1 (Fig. S3), calculated using Hammer's factors (f_c), confirms that there is little orientation change of the HDPE crystals. These results prove that the applied strain has not induced any change in the HDPE crystal orientation. Therefore, the conductive networks are mainly fixed in HDPE matrix (crystalline), leaving only nanotubes with small motion realm, such as increasing distance of neighboring nanotubes (Figs. 6b and 7b). This distance between nanotubes can be regard as the tunneling distance (D_t) [51] and its effect on electrical resistance of composites will be further discussed in Section 3.3.

Table 2
Summary of GF data concerning HDPE/MWCNT and HDPE/GNP composites after damage self-sensing measurements.

Sample	$0\sim\varepsilon_1$[a)] [%]	GF_1	$\varepsilon_1\sim\varepsilon_2$[b)] [%]	GF_2	$\varepsilon_2\sim\varepsilon_3$[c)] [%]	GF_3
S-CNT1	17.8	15.8	66.8	2.2	82.5	27.3
D-CNT1	20.9	43.3	47.9	15.1	56.1	403.3
D-CNT3	21.6	21.3	62.7	3.5	72.6	89.6
S-GNP3	9.4	23.5	–	–	–	–
S-GNP4	6.2	11.5	–	–	–	–
D-GNP12	3.8	12.2	–	–	–	–

[a),b)] and [c)] representing ε_1, ε_2 and ε_3 are shown below, respectively.

The gauge factor in the initial stage (GF_1) of D-CNT1 was estimated to be 43.3 (Table .2), which is about twice that of D-CNT3 (21.3). This can be attributed to a robust conductive network in the D-CNT3 system which has more MWCNTs. With respect to S-CNT1, it has quite a low GF_1 value (15.8). This is even lower than that of D-CNT3 in spite of higher content of MWCNTs. These results indicate how the different types of conductive network structure significantly influence the GF values of the composites. Unlike the composites with a DCN structure where the isolated and agglomerated MWCNTs (red dash circles in Fig. 6a and b) are uniformly distributed, the MWCNTs in a SCN structure are mainly accumulated at the interfaces of the HDPE phases and form denser conductive pathways with more contacts and entanglements (gray strip in Fig. 7a and b). This type of conductive network can better withstand applied strain, resulting in a lower GF_1 value compared to the DCN structure.

As strain increases from ε_1 to ε_2, the stress gradually declines and then levels off (light green background, Fig. 5). This is due to the deformation and destruction of some crystalline lamellae and is commonly referred to as the strain softening region [52]. More obvious orientation of polymer crystals happens based on significantly increasing f_c values when the specimens are further stretched up to ε_2 (Fig. S3). A decrease of about 5% in X_{XRD} (Fig. S2) supports the point that the crystals are being destroyed as deformation increases.

All the $\Delta R/R_0$ curves tend towards a "plateau" in this stage and the related GF_2 values are much lower compared to the previous stage. Such a plateau is

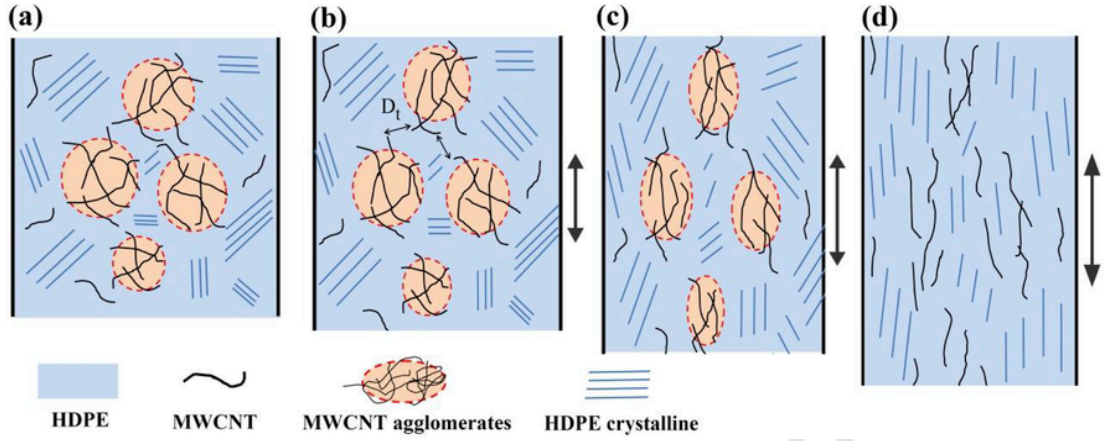

Fig. 6. Schematic of the conductive network evolution of HDPE/MWCNT composites with a DCN structure: (a) before stretching, (b) prior to yielding (0 to ε_1), (c) strain softening (ε_1 to ε_2), and (d) necking growth ($> \varepsilon_2$).

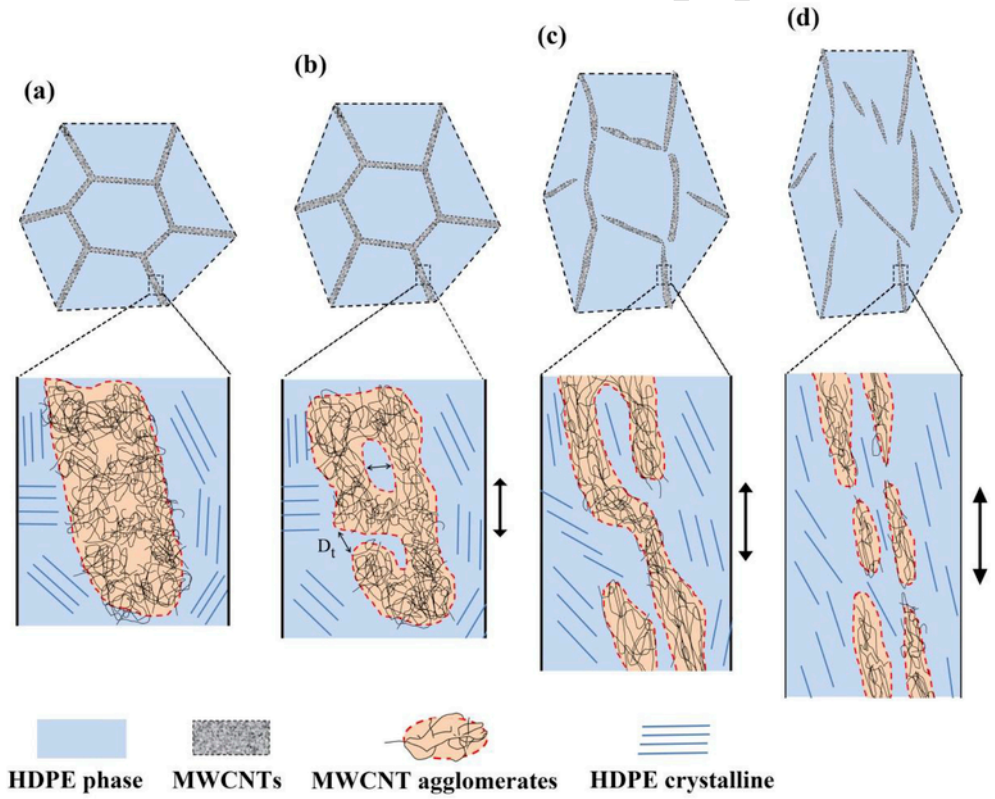

Fig. 7. Schematic of the conductive network evolution of HDPE/MWCNT composites with a SCN structure: (a) before stretching, (b) prior to yielding (0 to ε_1), (c) strain softening (ε_1 to ε_2), and (d) necking growth ($> \varepsilon_2$).

associated with the orientation of nanotubes induced by the deformation of the polymer crystals. As MWCNTs possess considerable flexibility owing to their 1-dimensional shape and high aspect ratio, the deformation of conductive networks may reach a balance between (1) the destruction of previous conductive pathways induced by nanotubes orientation and (2) reconstruction of new conductive pathways resulting from forming other new contacts of nanotubes (Figs. 6c and 7c). Thus, such a dynamically changing conductive network basically maintains the previous conductive ability and small variations in $\Delta R/R_0$ values (the plateau) are obtained during this stage of the tensile deformation process. In Fig. 5b, D-CNT1 has the highest $\Delta R/R_0$ value of about 1100 at the plateau due to a less stable conductive network. This is almost 3 and 2 times as much as that of S-CNT1 (340) and D-CNT3 (540), respectively. In addition, clear fluctuations in $\Delta R/R_0$ in the plateau region can be observed for S-CNT1 in Fig. 5a. This may be related to more intensive competition between destruction and rebuilding of conductive networks in the segregated structure.

At the end of the strain softening stage (denoted as ε_2), necking occurs and extends along the tensile direction with further stretching. In this "necking growth" stage, the f_c values (Fig. S3) and X_{XRD} (Fig. S2) of both D-CNT1 and S-CNT1 clearly increase. This indicates that HDPE crystals are further orientated and strain induced recrystallization occurs. In addition, the previous balance in destruction and rebuilding of conductive networks is broken with further orientation of nanotubes, and the destruction effect plays a dominant role. Therefore, all $\Delta R/R_0$ curves start to increase again (Fig. 5a–c, pink background). As $\Delta R/R_0$ rapidly increases in a large strain range after ε_2 (Fig. S4), the gauge factors (GF_3) of all specimens are calculated at the beginning range of this stage for quantitative analysis ($\varepsilon_2 < \varepsilon_3 < \varepsilon_2 + 15\%$). Likewise, D-CNT1

and S-CNT1 exhibit the highest (403.3) and lowest (27.3) GF_3 values respectively, and D-CNT3 shows a moderate GF_3 value of 89.6 (Table 2). The deformation of the conductive networks of D-CNT1 and S-CNT1 is quite different in this stage (illustrated in Figs. 6d and 7d). For the D-CNT1 sample, numerous nanotubes are disentangled and rearrange along the tensile direction (Fig. 8a). Some neighboring nanotubes could be further separated so that they cannot effectively form conductive pathways. For the S-CNT1 system, although the original net-like conductive networks have been largely deformed and disrupted (Fig. 8b), the nanotubes are still tightly entangled at the interfaces of the HDPE phases (Fig. 8c). Such a conductive network structure enables better retention of its electrical conductivity and results in a relatively low GF_3.

Finally, an abrupt increase in $\Delta R/R_0$ values is observed at the end region of all curves. This originates from: (1) fracture of the dumbbell specimens during tensile testing for S-CNT1 (Fig. S4a) and D-CNT3 (Fig. S4c), and (2) too high an electrical resistance to be measured by the picoammeter prior to the fracture (D-CNT1, Fig. S4b).

3.2.2. Damage self-sensing of HDPE/GNP composites

The HDPE/GNP composites exhibit more brittle mechanical behavior under tensile elongation than that of the HDPE/MWCNT composites with a consequent difference in their self-sensing behavior, as shown in Fig. 9. All the $\Delta R/R_0$ curves for the HDPE/GNP systems monotonously increase as strain increases until a sharp jump at the brittle fracture stage. Since the values of elongation at break are quite low, namely 9.4% for S-GNP3 (Figs. 9a) and 3.8% for D-GNP12 (Fig. 9c), their $\Delta R/R_0$ values (approximately 200% for S-GNP3) are far lower than those of the HDPE/MWCNT (reach to 10^6%) (Fig. S3).

As all the HDPE/GNP composites are brittle fractured prior to yielding, their GF_1 values are calculated from 0% to the strain at break (denoted as ε_1). One can see in Table 2 that the GF_1 value of S-GNP3 is higher than that of S-GNP4 (23.5 versus 11.5). This is mainly attributed to a less stable conductive network structure of the S-GNP3 with a lower GNP loading. Moreover, although the GNP loading of D-GNP12 is 3 times as much as that of S-GNP4, their GF_1 values are very close (approximately 12), indicating the higher stability of conductive networks in a segregated structure. These phenomena are consistent with those shown in HDPE/MWCNT systems.

3.3. Modeling and mechanism

As discussed above, the conductive network structures of the composites are not significantly deformed since the HDPE crystals barely change prior to yielding. The variation of $\Delta R/R_0$ values can be mainly attributed to the increase of distance between nanofillers (MWCNTs or GNPs), which is interpreted as the tunneling effect [43]. In order to further analyze this, a modeling study, derived from tunneling theory by Simmons [53], was carried out. The total resis-

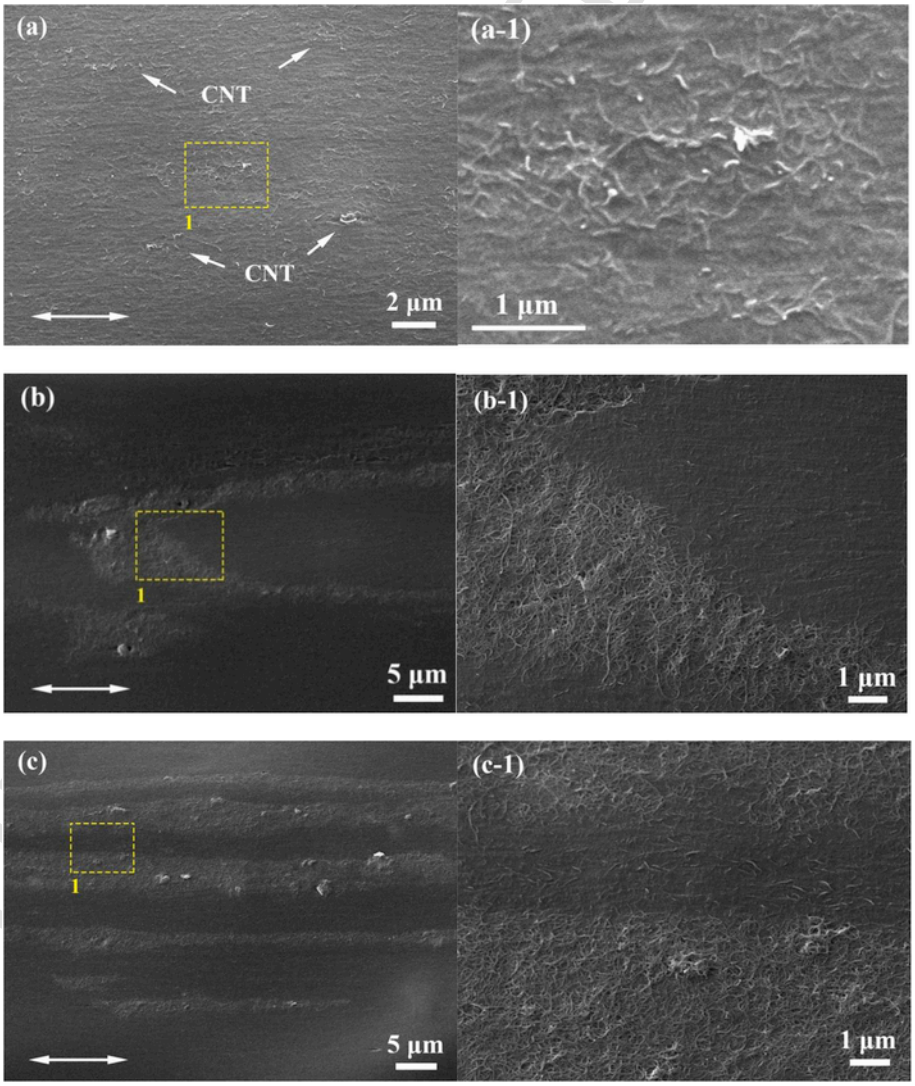

Fig. 8. SEM micrographs of HDPE/MWCNT composites with different conductive networks after stretching to a strain of 300%: (a) D-CNT1, (b, c) S-CNT1. The double-headed arrows represent the tensile direction.

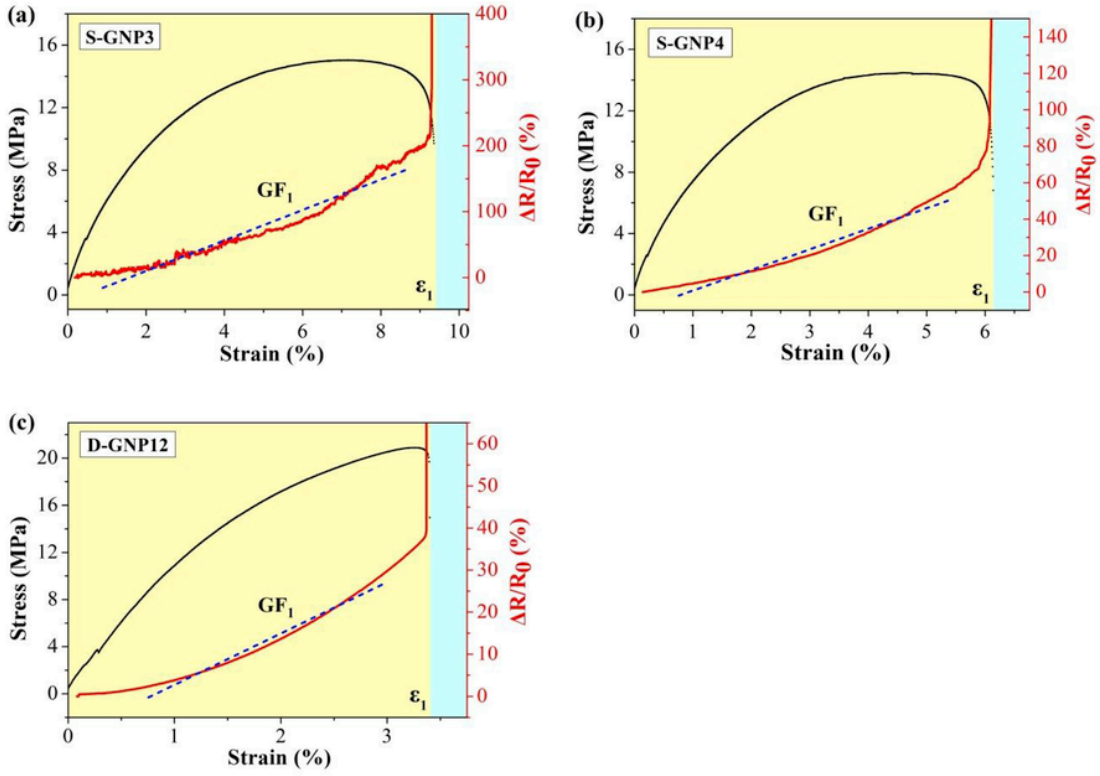

Fig. 9. Tensile stress and relative resistance change ($\Delta R/R_0$) versus strain of (a) S-GNP3, (b) S-GNP4, and (c) D-GNP12.

tance R of a sample can be represented by Equation (4)

$$R = \left(\frac{L}{N}\right)\left(\frac{8\pi hs}{3\gamma a^2 e^2}\right)\exp(\gamma s) \tag{4}$$

$$\gamma = \frac{4\pi\sqrt{2m\varphi}}{h} \tag{5}$$

where L is the number of particles forming a single conductive path, N is the number of conductive pathways, h is Planck's constant, sis the shortest distance between conductive particles, a^2 is the effective cross-section area, eis the electron charge, mis the electron mass, and φ is the height of the potential barrier between particles.

When the sample is strained, its electrical resistance will be altered due to separation of the conductive nanoparticles and changes in the inter-particle distance. The distance will vary linearly and proportionally with strain increases from s_0 to s, hence it can be expressed as follows:

$$s = s_0\left(1 + C\left(\frac{\Delta l}{l_0}\right)\right) = s_0(1 + C\varepsilon) \tag{6}$$

where l_0 is the initial length of the sample, Δl is the deformation length, ε is tensile strain elongation, and C is a constant depending on material systems.

The non-linear rate of resistivity increase at larger strains indicates a non-linear response for the number of conductive pathways (N) at large strain. This can be represented by Equation (7):

$$N = \frac{N_0}{\exp\left(M\varepsilon + W\varepsilon^2 + U\varepsilon^3 + V\varepsilon^4\right)} \tag{7}$$

where M, W, U, V are constants.

Substitution of Equations (6) and (7) into Equation (4) gives Equation (8):

$$R = B(1+C\varepsilon)\exp\left[A+(M+AC)\varepsilon+W\varepsilon^2+U\varepsilon^3+V\varepsilon^4\right] \tag{8}$$

where $A = \gamma S_0$, $B = \frac{8\pi hns_0}{3\gamma N_0^2 e^2 a^2}$, and n is the total number of conductive particles (n = L × N).

Fig. 10 shows that the experimental data are well represented by this tunneling model, and the related fitting parameters are listed in Table S1. The change of tunneling distance (change of TD) and change of conductive pathways (change of CP) of HDPE/MWCNT and HDPE/GNP composites are plotted against strain as shown in Fig. 11. In the HDPE/MWCNT system, the tunneling distance of MWCNTs in D-CNT1 increases much more significantly than that in S-CNT1 (Fig. 11a), which confirms that the conductive network with the dispersed structure is less robust compared with the segregated structure. Also, the number of conductive pathways in S-CNT1 decreases more slowly with strain than that in D-CNT3 (Fig. 11c). Likewise, it can be observed in the HDPE/GNP composites that the number of conductive pathways in S-GNP3 and S-GNP4 decreases more slowly than that in D-GNP12 (Fig. 11d). However, Fig. 11b shows that the tunneling distance of GNPs in D-GNP12 increases at the lowest rate relative to S-GNP3 an S-GNP4, which is mainly attributed to much higher GNP loading.

3.4. Tensile properties

The tensile properties of HDPE/MWCNT and HDPE/GNP composites were obtained from the in situ mechanical-electrical measurement system, and the data are shown in Fig. 12 and in Table 3. Significant effects of nanoparticle loading on tensile properties can be observed in the stress-strain curves (Fig. 12a). In Fig. 12b, there is a moderate increase in Young's modulus with the addition of MWCNT and a more noticeable increase with GNP addition (90% increase for a loading of 12 wt.%, Table 3). This can be attributed to the higher modulus of nanoparticles relative to the soft HDPE matrix and to the higher aspect ratio of GNPs relative to MWCNTs [54]. The elongation at break (ε_b) is

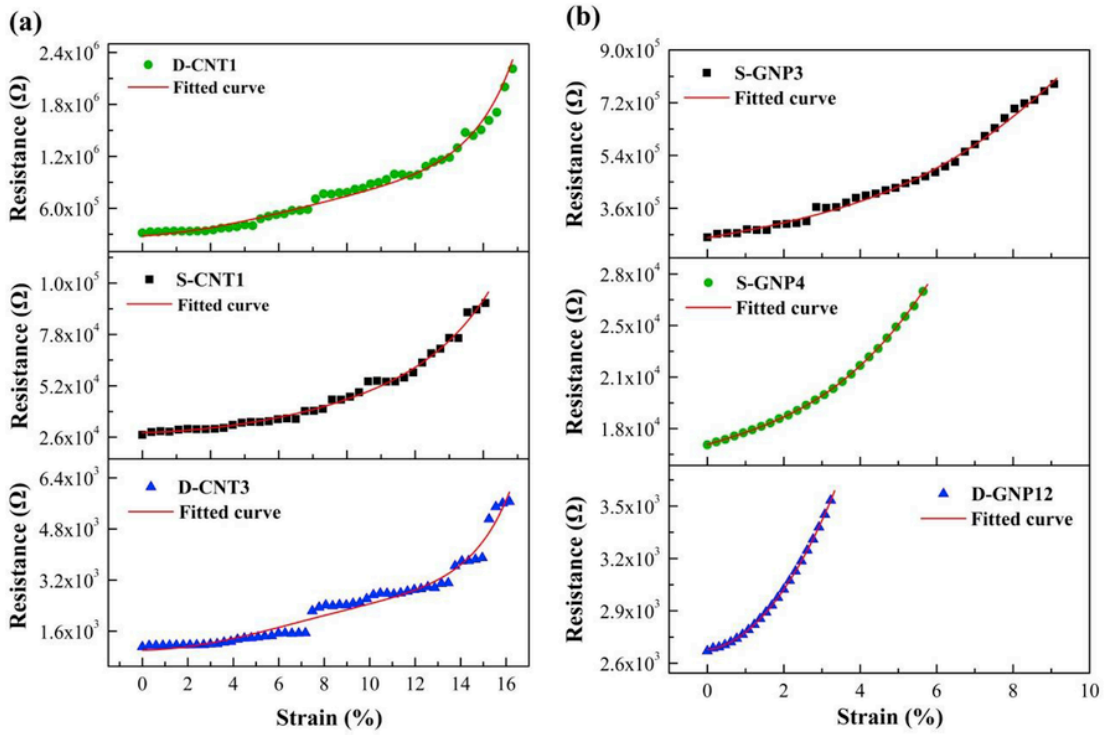

Fig. 10. Experimental (dots) and theoretical (red solid lines) results for the electrical resistance-strain relationship of (a) HDPE/MWCNT composites, (b) HDPE/GNP composites. (For interpretation of the references to colour in this figure legend, the reader is referred to the Web version of this article.)

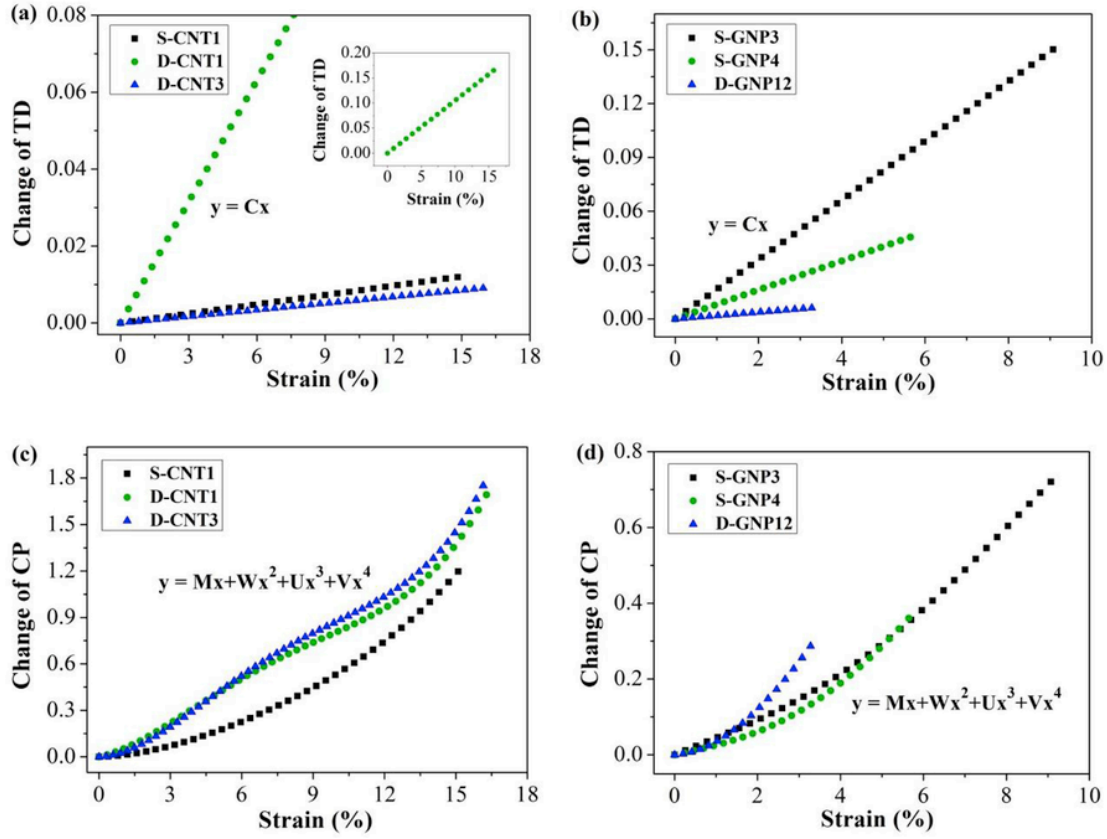

Fig. 11. Change of the tunneling distance of (a) HDPE/MWCNT and (b) HDPE/GNP and change of the conductive pathway of (c) HDPE/MWCNT and (d) HDPE/GNP composites as a function of strain.

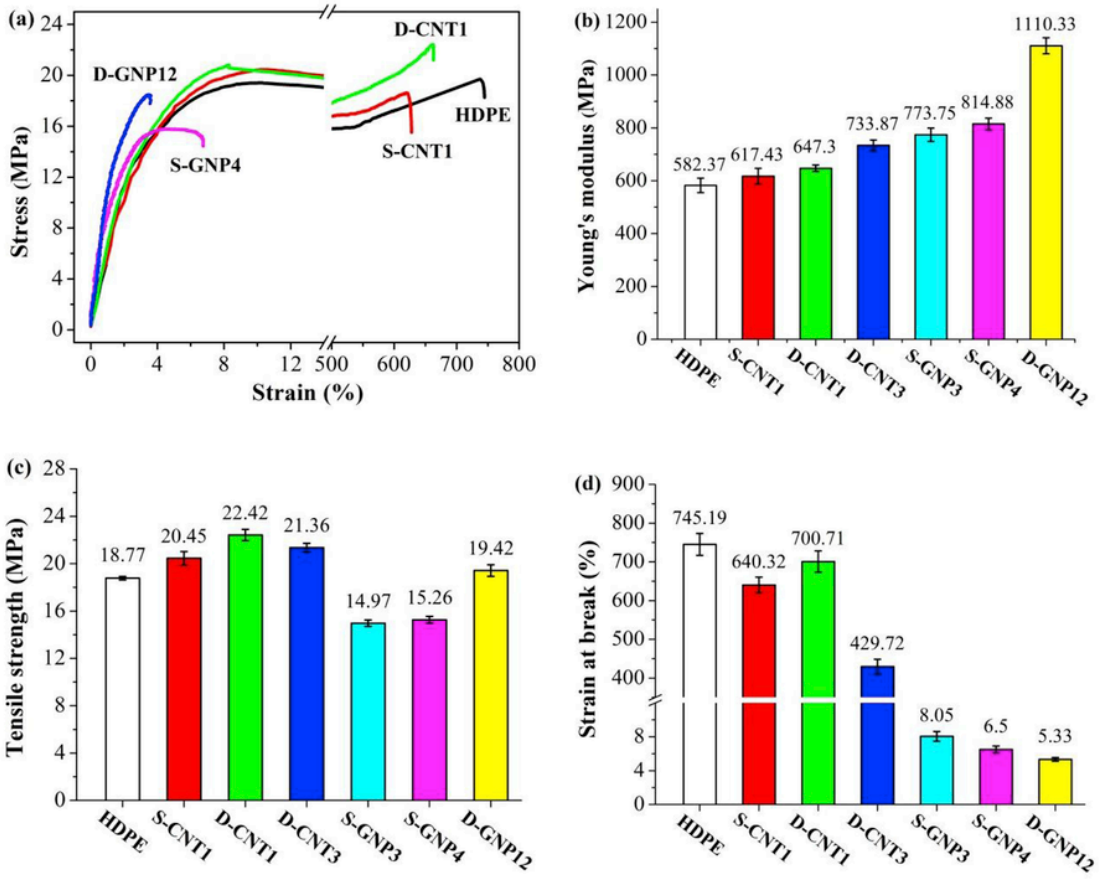

Fig. 12. Tensile properties of HDPE composites as a function of carbon nanofiller loading and conductive network structures.

Table 3
Effect of nanofillers and conductive network structures on tensile properties of HDPE composites.

Sample	ΔE[%]	$\Delta\sigma_T$[%]	$\Delta\varepsilon_b$[%]
S-CNT1	6.0	9.0	−14.1
D-CNT1	11.1	19.4	−6.0
D-CNT3	26.0	13.8	−42.3
S-GNP3	32.9	−20.2	−98.9
S-GNP4	39.9	−18.7	−99.1
D-GNP12	90.7	3.5	−99.3

only very slightly reduced for MWCNT addition of 1 wt.% thus resulting in an increase in tensile strength for these materials. As the loading of MWCNTs increases to 3 wt.%, the value of ε_b decreases but tensile strength is still greater than the unfilled material. The addition of GNPs has a more dramatic impact on elongation at break and reduces it substantially relative to the MWCNTs. These negative effects of GNPs on elongation and toughness can be attributed to the 2-dimensional, flake-like structure and high aspect ratio of GNPs which leads to the formation of agglomerates induced by the strong Van der Waals forces exerted between GNP sheets with high surface areas. These agglomerates act as stress concentrators and lead to microcracking under deformation, leading to brittle fracture of the tensile specimens.

The tensile properties are also related to the conductive network structure type, namely SCN and DCN. In Fig. 12d, ε_b of S-CNT1 is measured to be 640.3% which is lower than that of D-CNT1 (700.7%). This can be attributed to two factors. Firstly, the relatively random and uniform dispersion of MWCNT agglomerates in the composites formed with a DCN structure increase the physical crosslink points and enhanced stress transfer between the polymer matrix and nanofillers, yielding superior Young's modulus and tensile strength. Secondly, for composites with a SCN structure, MWCNTs are segregated by HDPE particles into strip-like pathways, in which HDPE may not have completely permeated. As a result, small holes between the nanotubes may serve as microcracks and defects speeding up the progress of fracture.

4. Conclusions

This study primarily examined the electrical properties and damage self-sensing behavior of HDPE/MWCNT and HDPE/GNP composites with different conductive network structures. The electrical conductivities of all prepared composites improved as nanofiller contents rose, and this improvement in conductivity was greater in the segregated conductive network structure, where more efficient conductive pathways formed. The results also showed that nanofiller type (MWCNTs and GNPs) and conductive network structures (DCN and SCN) significantly affect the damage self-sensing behavior of the composites. Firstly, three typical stages corresponding to the region prior to yielding, strain softening and necking growth were mirrored by changes in $\Delta R/R_0$ of the HDPE/MWCNT composites during tensile deformation. Secondly, for the HDPE/MWCNT composites with a SCN structure, MWCNTs accumulated in the narrow region of the HDPE phase boundaries to form robust conductive networks, where nanotubes/agglomerates were tightly entangled. This conductive network yielded lower GF and $\Delta R/R_0$ values (plateau). Compared to the SCN structure, the conductive network of the HDPE/MWCNT system with a DCN structure was more sensitive to tensile deformation (high GF values) due to weaker conductive networks with insufficient connections between nanotubes/agglomerates. Thirdly, the evolution of conductive networks in the composites can be affected by the deformation of HDPE crystals, which is confirmed by the changes of the crystallinity and the orientation degree of HDPE crystals under different tensile strains. Fourthly, the self-damage sensing behaviors of HDPE/GNP composites showed a quasi-linear increase (ε <10%) in $\Delta R/R_0$ followed by an abrupt jump. This can be explained

by brittle fracture behavior in the HDPE/GNP composites. In addition, a modeling study based on tunneling theory was conducted to further analyze the mechanism, and the results show a good reflection of the experimental data. Also, MWCNTs positively affected the tensile strength and modulus of the HDPE while the GNPs led to high Young's modulus but a more brittle behavior. This study provides some important information for the development of smart structural materials.

Acknowledgements

This work was financially supported by Sichuan Science and Technology Program (2017HH0086, 2017JY0152), Education Department of Sichuan Province (17ZB0462), Open Experimental Program of SWPU (KSZ17123), and Innovative Research Team of SWPU (2017CXTD01).

Appendix A. Supplementary data

Supplementary data to this article can be found online at https://doi.org/10.1016/j.polymer.2018.11.007.

References

[1] M. Amjadi, K.U. Kyung, I. Park, M. Sitti, Stretchable, skin-mountable, and wearable strain sensors and their potential application: a review, Adv. Funct. Mater. 26 (2016) 1678–1698.
[2] Y.J. Yim, S.J. Park, Electromagnetic interference shielding effectiveness of high density polyethylene composites reinforced with multi-walled carbon nanotubes, J. Ind. Eng. Chem. 21 (2015) 155–157.
[3] J.D. Shi, X.M. Li, H.Y. Cheng, Z.J. Liu, L.Y. Zhao, T.T. Yang, et al., Graphene reinforced carbon nanotube networks for wearable strain sensors, Adv. Funct. Mater. 26 (2016) 2078–2084.
[4] W. Lan, Y.X. Chen, Z.W. Yang, W.H. Han, J.Y. Zhou, Y. Zhang, et al., Ultraflexible transparent film heater made of Ag nanowire/PVA composite for rapid-response thermotherapy pads, ACS Appl. Mater. Interfaces 9 (2017) 6644–6651.
[5] X. Zhou, L. Zhu, L. Fan, H. Deng, Q. Fu, The fabrication of highly stretchable, washable, wearable, water repellent strain sensors with multi-stimuli sensing ability, ACS Appl. Mater. Interfaces 10 (37) (2018) 31655–31663.
[6] W.J. Na, J.H. Byun, M.G. Lee, W.R. Yu, In-situ damage sensing of woven composites using carbon nanotube conductive networks, Composites Part A 77 (2015) 229–236.
[7] Y. Wang, R. Chang, G. Chen, Strain and damage self-sensing properties of carbon nanofibers/carbon fiber-reinforced polymer laminates, Adv. Mech. Eng. 9 (2017) 1–11.
[8] L.Y. Duan, S.R. Fu, H. Deng, Q. Zhang, K. Wang, F. Chen, et al., The resistivity-strain behavior of conductive polymer composites: stability and sensitivity, J. Mater. Chem. 2 (2014) 17085–17098.
[9] V. Trappe, K.W. Harbich, Intralaminar fatigue behaviour of carbon fibre reinforced plastics, Int. J. Fatig. 28 (2006) 1187–1196.
[10] M. Todd, M. Yeager, C. Key, W. Gregory, Assessment of embedded fiber brag gratings for structural health monitoring of composites, In Struct. Health Monit. 16 (2017) 262–275.
[11] V. Janapati, F. Kopsaftopoulos, F. Li, S.J. Lee, F.K. Chang, Damage detection sensitivity characterization of acousto-ultrasound-based structural health monitoring techniques, Struct. Health Monit. 15 (2016) 143–161.
[12] A. Maaroufi, K. Haboubi, A.E. Amarti, F. Carmona, Electrical resistivity of polymeric matrix loaded with nickel and cobalt powders, J. Mater. Sci. 39 (2004) 265–270.
[13] J. Rams, M. Sánchez, A. Ureña, A. Jiménezsuárez, M. Campo, A. Güemes, Use of carbon nanotubes for strain and damage sensing of epoxy-based composites, Int. J. Soc. Netw. Min. 3 (2012) 1–10.
[14] W. Li, A. Dichiara, J. Bai, Carbon nanotube–graphene nanoplatelet hybrids as high-performance multifunctional reinforcements in epoxy composites, Compos. Sci. Technol. 74 (2013) 221–227.
[15] W.L. Gao, Y. Zheng, J.B. Shen, S.Y. Guo, Electrical properties of polypropylene-based composites controlled by multilayered distribution of conductive particles, ACS Appl. Mater. Interfaces 7 (3) (2015) 1541–1549.
[16] V.K. Vadlamani, V.B. Chalivendra, A. Shukla, S. Yang, Sensing of damage in carbon nanotubes and carbon black-embedded epoxy under tensile loading, Polym. Compos. 33 (2012) 1809–1815.
[17] Z. Starý, Simultaneous electrical and rheological measurements on melts of conductive polymer composites under elongation, Polymer 55 (2014) 5608–5611.
[18] Y. Zhou, Y. Zhou, H. Deng, Q. Fu, A novel route towards tunable piezoresistive behavior in conductive polymer composites: addition of insulating filler with different size and surface characteristics, Composites Part A 96 (2017) 99–109.
[19] S.D. Zheng, J. Deng, L.Q. Yang, D.Q. Ren, S.L. Huang, W. Yang, et al., Investigation on the piezoresistive behavior of high-density polyethylene/carbon black films in the elastic and plastic regimes, Compos. Sci. Technol. 97 (2014) 34–40.
[20] A. Todoroki, K. Yamada, Y. Mizutani, Y. Suzuki, R. Matsuzaki, Impact damage detection of a carbon-fibre-reinforced-polymer plate employing self-sensing time-domain reflectometry, Compos. Struct. 130 (2015) 174–179.
[21] L.M. Chiacchiarelli, M. Rallini, M. Monti, D. Puglia, J.M. Kenny, L. Torre, The role of irreversible and reversible phenomena in the piezoresistive behavior of graphene epoxy nanocomposites applied to structural health monitoring, Compos. Sci. Technol. 80 (2013) 73–79.
[22] N. Kalashnyk, E. Faulques, J.S. Thomsen, L.R. Jensen, J.C.M. Rauhe, R. Pyrz, Monitoring self-sensing damage of multiple carbon fiber composites using piezoresistivity, Synth. Met. 224 (2017) 56–62.
[23] Y. Mouhamad, T. Mortensen, A. Holder, A.R. Lewis, T.G.G. Maffeis, D. Deganello, High performance tunable piezoresistive pressure sensor based on direct contact between printed graphene nanoplatelet composite layers, RSC Adv. 6 (2016) 125206–125210.
[24] D.J. Kwon, Z.J. Wang, J.Y. Choi, Damage sensing and fracture detection of CNT paste using electrical resistance measurements, Composites Part B 90 (2016) 386–391.
[25] M.Z. Ji, H. Deng, D.X. Yan, X.Y. Li, L.Y. Duan, Q. Fu, Selective localization of multi-walled carbon nanotubes in thermoplastic elastomer blends: an effective method for tunable resistivity–strain sensing behavior, Compos. Sci. Technol. 92 (92) (2014) 16–26.
[26] K. Ke, P. Potschke, N. Wiegand, B. Krause, B. Voit, Tuning the network structure in poly (vinylidene fluoride)/carbon nanotube nanocomposites using carbon black: towards improvements of conductivity and piezoresistive sensitivity, ACS Appl. Mater. Interfaces 8 (2016) 14190–14199.
[27] D. Xiang, L. Wang, Y.H. Tang, E. Harkin-Jones, C.X. Zhao, Y.T. Li, Processing-property relationships of biaxially stretched binary carbon nanofiller reinforced high density polyethylene nanocomposites, Mater. Lett. 209 (2017) 551–554.
[28] F. Nanni, B. Mayoral, F. Madau, G. Montesperelli, T. McNally, Effect of MWCNT alignment on mechanical and self-monitoring properties of extruded PET-MWCNT nanocomposites, Compos. Sci. Technol. 72 (2012) 1140–1146.
[29] X.F. Sánchez-Romate, R. Moriche, A. Jiménez-Suárez, M. Sánchez, S.G. Prolongo, A. Güemes, et al., Highly sensitive strain gauges with carbon nanotubes: from bulk nanocomposites to multifunctional coatings for damage sensing, Appl. Surf. Sci. 424 (2017) 213–221.
[30] A. Baltopoulos, N. Athanasopoulos, I. Fotiou, A. Vavouliotis, Sensing strain and damage in polyurethane/MWCNT nano-composite foams using electrical measurements, Express Polym. Lett. 7 (2013) 40–54.
[31] J.M. Zhu, J.B. Shen, S.Y. Guo, H.J. Sue, Confined distribution of conductive particles in polyvinylidene fluoride-based multilayered dielectrics: toward high permittivity and breakdown strength, Carbon 84 (1) (2015) 355–364.
[32] S. Zhang, H. Deng, Q. Zhang, Q. Fu, Formation of conductive networks with both segregated and double-percolated characteristic in conductive polymer composites with balanced properties, ACS Appl. Mater. Interfaces 6 (2014) 6835–6844.
[33] H. Pang, D.X. Yan, Y. Bao, J.B. Chen, C. Chen, Z.M. Li, Super-tough conducting CNT/UHMWPE composites with segregated and double-percolated structure, J. Mater. Chem. 22 (2012) 23568–23575.
[34] H.J. Zhou, H. Deng, L. Zhang, Z.Q. Wu, S. Deng, W.X. Yang, et al., Toward multi-functional polymer composites through selectively distributing functional fillers, Composites Part A 82 (2016) 20–33.
[35] Y. Lin, X.C. Dong, S.Q. Liu, S. Chen, Y. Wei, L. Liu, Graphene-elastomer composites with segregated nanostructured network for liquid and strain sensing application, ACS Appl. Mater. Interfaces 8 (2016) 24143–24151.
[36] R. Patra, S. Suin, D. Mandal, B.B. Khatua, Sequential mixing as effective method in the reduction of percolation threshold of multiwall carbon nanotube in poly(methylmethacrylate)/high-density poly(ethylene)/MWCNT nanocomposites, J. Appl. Polym. Sci. 131 (2014) 40235–40247.
[37] M. Wang, K. Zhang, X.X. Dai, Y. Li, J. Guo, H. Liu, et al., Enhanced electrical conductivity and piezoresistive sensing in multi-wall carbon nanotubes/polydimethylsiloxane nanocomposites via the construction of a self-segregated structure, Nanoscale 9 (2017) 11017–11026.
[38] R.H. Olley, D.C. Bassett, An improved permanganic etchant for polyolefines, Polymer 23 (1982) 1707–1710.
[39] D. Stauffer, A. Aharony, Introduction to percolation theory, Phys. Today 40 (1986) 425–478.
[40] H. Deng, L. Lin, M.Z. Ji, S.M. Zhang, M.B. Yang, Q. Fu, Progress on the morphological control of conductive network in conductive polymer composites and the use as electroactive multifunctional materials, Prog. Polym. Sci. 39 (2014) 627–655.
[41] D. Xiang, L. Wang, Y.H. Tang, C.J. Hill, B. Chen, E. Harkin-Jones, Reinforcement effect and synergy of carbon nanofillers with different dimensions in high density polyethylene based nanocomposites, Int. J. Mater. Res. 108 (2017) 322–334.
[42] H. Liu, J.C. Cheng, W.J. Huang, K. Dai, G.Q. Zheng, C.T. Liu, et al., Electrically conductive strain sensing polyurethane nanocomposites with synergistic carbon nanotubes and graphene bifillers, Nanoscale 8 (2016) 12977–12989.
[43] D. Stauffer, A. Aharony, Introduction to Percolation Theory, second ed., Taylor and Francis, Washington, DC, 199252.
[44] H. Koerner, W. Liu, M. Alexander, P. Mirau, H. Dowty, R.A. Vaia, Polymer 46 (2005) 4405–4420.
[45] M.J. Arlen, D. Wang, J.D. Jacobs, R. Justice, A. Trionfi, J.W.P. Hsu, et al., Thermal-electrical character of in situ synthesized polyimide-grafted carbon nanofiber composites, Macromolecules 41 (2015) 8053–8062.
[46] S. Vionnet-Menot, C. Grimaldi, T. Maeder, S. Strässler, P. Ryser, Tunneling-percolation origin of nonuniversality: theory and experiments, Phys. Rev. B 71 (2005), 064201.
[47] M. Mohiuddin, S.V. Hoa, Temperature dependent electrical conductivity of CNT-PEEK composites, Compos. Sci. Technol. 72 (2011) 21–27.
[48] Q. Chen, D. Xiang, L. Wang, Y.H. Tang, E. Harkin-Jones, C.X. Zhao, et al., Facile fabrication and performance of robust polymer/carbon nanotube coated spandex fibers for strain sensing, Composites Part A 112 (2018) 186–196.
[49] J.H. Du, L. Zhao, Y. Zeng, L.L. Zhang, F. Li, P.F. Liu, et al., Comparison of electrical properties between multi-walled carbon nanotube and graphene nanosheet/high density polyethylene composites with a segregated network structure, Carbon 49 (2011) 1094–1100.
[50] Z. Spitalsky, D. Tasis, K. Papagelis, C. Galiotis, Carbon nanotube-polymer composites: chemistry, processing, mechanical and electrical properties, Prog. Polym. Sci. 35 (2010) 357–401.

[51] N. Hu, Z. Masuda, C. Yan, G. Yamamoto, H. Fukunaga, T. Hashida, The electrical properties of polymer nanocomposites with carbon nanotube fillers, Nanotechnology 19 (2008) 215701.
[52] K. Chen, K.S. Schweizer, Theory of Yielding, Strain softening, and steady plastic flow in polymer glasses under constant strain rate deformation, Macromolecules 44 (2011) 3988–4000.
[53] J.G. Simmons, Generalized formula for the electric tunnel effect between similar electrodes separated by a thin insulating film, J. Appl. Phys. 34 (1963) 1793–1803.
[54] D. Das, B.K. Satapathy, Microstructure-rheological percolation-mechanical properties correlation of melt-processed polypropylene-multiwall carbon nanotube nanocomposites: influence of matrix tacticity combination, Mater. Chem. Phys. 147 (2014) 127–140.